Acta Cryst. (1996). A52, 614–620

X-ray Back-Diffraction Profiles with an Si (111) Plate

C. CUSATIS,[a]* D. UDRON,[a] I. MAZZARO,[a] C. GILES[b]† AND H. TOLENTINO[c]

[a]*Departamento de Física, Universidade Federal do Paraná, CP 19091, 81531-990 Curitiba (PR), Brasil,* [b]*European Synchrotron Radiation Facility (ESRF), BP 220, F-38043 Grenoble CEDEX, France, and* [c]*Laboratório Nacional de Luz Síncrotron (LNLS) CNPq, CP 6192, 13081-970 Campinas (SP), Brasil. E-mail: cusatis@fisica.ufpr.br*

(Received 8 September 1995; accepted 15 January 1996)

Abstract

A two- and, alternatively, a four-crystal monochromator were used for simultaneous measurements of the profiles backward (*h*) and forward (*o*) diffracted by a thin Si (111) crystal plate for diffraction angles up to exactly 90° at DCI–LURE (Orsay). It is shown that the set-up with a four-crystal monochromator allows the characterization of the back-diffraction region for any crystal plate reflection. Asymmetry and full width at half-maximum (FWHM) of the experimental backward-diffraction profiles are analyzed. Possible simultaneous diffractions occurring near 90° incidence, giving extra peaks in the forward-diffracted profiles, are studied. The good contrast of the *o*-beam profiles suggests that the back-diffracted *o* beam could be used as a highly monochromatic beam.

1. Introduction

The X-ray near-back-diffraction regime is especially interesting for X-ray optics: it combines very large angular acceptance (the Darwin width can be orders of magnitude bigger than the usual values when the Bragg angle approaches 90°) with high energy resolution (Kohra & Matsushita, 1972; Brümmer, Höche & Nieber, 1979; Caticha & Caticha-Ellis, 1982; Graeff & Materlik, 1982; Hashizume & Nakahata, 1988). In this diffraction regime, the energy resolution can be as good as the intrinsic energy resolution and the goniometry is much less sensitive than for usual Bragg angles. These special characteristics make the back-diffraction regime an excellent candidate for high-performance optical elements with respect to energy resolution and intensity.

X-ray back diffraction can be advantageously applied to high-resolution inelastic scattering (Dorner, Burkel & Peisl, 1986; Schülke, 1989; Hofmann, Kalus & Schmelzer, 1992), standing waves in non-perfect crystals (Woodruff *et al.*, 1987) and high-resolution or spin-dependent X-ray absorption spectroscopy (Hämäläinen, Siddons, Hastings & Berman, 1991; Hämäläinen *et al.*, 1992). X-ray back diffraction was suggested for the construction of X-ray Fabry–Perot interferometers (Steyerl & Steinhauser, 1979) and cavities for X-ray lasers (Denne, 1978). Nevertheless, to the best of our knowledge, few experimental studies of this diffraction regime exist until now (Graeff & Materlik, 1982; Kushnir & Suvorov, 1986; Stetsko, Kshevetskii & Mikhailyuk, 1988; Kondrashkina, Novikov & Stepanov, 1989; Kushnir & Suvorov, 1989; Nakahata, Hashizume, Oshima & Kawamura, 1989; Giles, 1991; Giles & Cusatis, 1991; Stepanov, Kondrashkina & Novikov, 1991; Giles & Cusatis, 1992), probably due to the difficulties inherent in back-diffraction geometry.

An experimental set-up suitable for measurement of back-diffraction profiles using a two- and, alternatively, a four-crystal monochromator, is presented in the first section of this paper. This set-up allows simultaneous measurement of the backward-diffracted and forward-diffracted profiles for a thin crystal at diffraction angles up to exactly 90°. First measurements made with a silicon (111) plate are presented and discussed in the second section.

2. Experiment

Performing back-diffraction experiments is somewhat difficult since the backward-diffracted *h* beam (and, for sufficiently thin samples, the forward-diffracted *o* beam), which propagates very close to or in the same direction as the incident beam, has to be detected. In general, the back-diffracted *h* beam is detected at long distances from the crystal in order to obtain spatial separation from the incident beam. The major inconvenience is that it requires long X-ray-source-to-sample distances (Graeff & Materlik, 1982; Dorner, Burkel & Peisl, 1986; Hofmann, Kalus & Schmelzer, 1992; Sette, 1993). Moreover, such a set-up does not allow detection at exactly 90°. Diffraction profiles at angles closer to 90° can be obtained, with set-ups of a largely reduced dimension, if a first-crystal reflection is used between the X-ray source and the sample (Kushnir & Suvorov, 1986; Stetsko, Kshevetskii & Mikhailyuk, 1988; Giles & Cusatis, 1992).

Another way to detect the back-diffracted *h*-beam profiles is to simultaneously measure the incident and back-diffracted beams, both going through the same detector but, naturally, in opposite directions, with a detector interfering weakly with the incident beam, en-

† Present address: LNLS, CP 6192, 13081-970 Campinas (SP), Brasil.

suring a good contrast between the diffracted peak intensity and the constant intensity due to the incident beam. This solution was used for studies of the back-diffraction profiles in Cu (111) with a photoemissive grid simultaneously measuring the incident and diffracted h beams with a contrast of 22% (Nakahata, Hashizume, Oshima & Kawamura, 1989). For the experiments reported here, an ionization chamber was used to detect the h-beam profiles. A better contrast, at most 50%, between the diffracted beam and the incident beam is obtained if the energy resolution of the incident beam is comparable with the energy resolution of the reflection of the back-diffracting crystal. For sufficiently thin crystals, the profile of the forward-diffracted o beam can also be detected (Giles & Cusatis, 1991). For the o beam, the contrast depends on the Borrmann effect and varies with sample thickness.

Experiments were done at the D45 beamline of DCI, the 1.85 GeV synchrotron source of LURE (Orsay, France), with 300 mA initial positron current in the ring. A two-crystal and, alternatively, a four-crystal monochromator with a vertical plane of diffraction delivered a monochromatized incident beam on the Si (111) sample (see Fig. 1).

The back-diffracting sample was a dislocation-free 380 μm thick Si (111) plate. The plate was mounted on a goniometer vertical axis driven by a step motor. A pre-orientation of the back-diffracting sample plate in the incident beam was achieved using photographic films and the plate was set perpendicular to the incident beam in the vertical plane within 1 mrad. When the incident angle approaches 90°, the diffraction profile becomes very sensitive to the temperature and the crystal temperature must be controlled. For a temperature variation ΔT of a crystal with linear thermal expansion coefficient α_T, the variation $\Delta\theta$ of the angle of the diffraction profile (called here 'diffraction angle') is

$$\Delta\theta = -\Delta T \alpha_T \tan\theta. \quad (1)$$

For $\Delta T = 1$ K in a silicon crystal at room temperature, $\Delta\theta$ is about 30″ at 89.0° and 60″ at 89.5°. In these experiments, the temperature of the Si plate was controlled to 1 K precision. The diffraction profile for a given temperature of the plate was recorded by rotating the plate around a vertical axis, with angular steps varying from 30 to 45″. Diffraction profiles with different diffraction angles were collected by keeping the incident-beam energy fixed and varying the plate temperature.

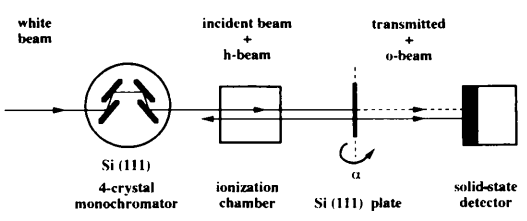

Fig. 1. Experimental set-up with the 4C monochromator for simultaneous measurement of the h-beam and o-beam profiles in the back-diffraction regime. The incident beam, o beam and h beam are shown separated for clarity. The silicon plate is rotated around a vertical axis parallel to the diffraction plane of the monochromator.

The h-beam profiles, added to the incident-beam background, were detected by an ionization chamber filled with air, allowing measurements with diffraction angles up to exactly 90°. The forward-diffracted o-beam profiles of the thin Si plate added to the purely transmitted beam were detected simultaneously by a scintillation detector, which recorded the intensity scattered by the beam air path, and by an Si(Li) solid-state detector intercepting the incident beam, with aluminium foils (200 μm) to attenuate the incident beam up to the operational rate of the solid-state detector.

The incident beam was monochromatized to $\Delta E/E = 10^{-5}$ in order to have good contrast for the back-diffraction profiles from the thin silicon plate. This energy resolution was achieved using two different monochromator set-ups: a two-crystal monochromator in a (+, −) non-dispersive mode operating near back diffraction and a four-crystal monochromator operating in a (+, −, −, +) dispersive mode at usual angles. In the dispersive mode, and in the non-dispersive mode with typical incident-beam divergence, the energy resolution is mainly defined by the intrinsic part $(\Delta E/E)_{\text{int}}$, the contribution to the energy resolution due to the energy width (ΔE_{int}) of the intrinsic diffraction profile. The intrinsic energy resolution $(\Delta E/E)_{\text{int}}$ is independent of the diffraction angle.

The temperature sensitivity of the monochromator is high: if the relative temperature between two previously tuned crystals of the monochromator varies by ΔT, and if $|\Delta T| \geq [(\Delta E/E)_{\text{int}} (\alpha_T)^{-1}]$, the reflection will be lost; that is, if $\Delta T \geq 55$ K for the Si 111 reflection at room temperature and if $\Delta T \geq 2$ and 0.15 K, respectively, for Si 444 and Si 777 reflections. In these experiments, the monochromator crystals were not temperature controlled and the temperature variation of the monochromator crystals during an angular scan of the plate was estimated to be less than 0.5 K.

2.1. *The two-crystal- (2C-) monochromator configuration*

A two-crystal monochromator with one rotation and two translations in the boomerang geometry was used (Corrêa, Tolentino, Craievich & Cusatis, 1991), with a pair of Si (111) crystals. The unusual feature of this monochromator was the utilization of monolithic mechanics with elastic translators, giving fast angular positioning and tuning between the two crystals, with very good stability and reproducibility (Tolentino, Durr, Mazzaro, Udron & Cusatis, 1995). Fine tuning in a range of 70″ was achieved by using a coil and a magnet on the

second-crystal holder. The design of the monochromator allowed it to be used at Bragg angles very close to 90°.

In this configuration, the reflection was the same for the monochromator and for the plate in order to match the incident energies selected by the monochromator with energies back diffracted by the plate. The two Si (111) crystals of the monochromator were set at a Bragg angle around 88.95°. For a 2*C* monochromator, the divergence of the outgoing beam is equal to the divergence of the incident beam. The incident-beam divergence was determined basically by the source and slit dimensions, and was approximately 0.25 (*V*) × 0.5 mrad (*H*).

In principle, all the *hhh* harmonics delivered by the 2*C* monochromator could be diffracted by the plate. The harmonic composition of the delivered beam was analyzed with a solid-state detector. The rocking curves for each harmonic were obtained by varying the angle of the second crystal of the monochromator. The angular range was limited owing to the maximum allowed current in the coil used for elastic adjustment of the second-crystal angle.

The 111 harmonic (E_{111} = 1.98 keV) was totally absorbed by the Be windows of the beam line and by the air (1 m) present between the monochromator and the Si plate. The 333 harmonic (E_{333} = 5.93 keV) was also reduced drastically and could not be detected mainly due to the attenuation in the aluminium foils in front of the solid-state detector. For the DCI emission spectra (critical energy 3.7 keV) and with these absorbers, it was expected that the 444 harmonic (E_{444} = 7.91 keV) should have much lower intensity than the higher harmonics. The monochromator was not perfectly aligned (the angle φ between the two crystals in the plane perpendicular to the vertical diffraction plane was estimated as 0.5–1°). Owing to this slight misalignment, the higher harmonic intensities were reduced and, for the higher harmonics, the angular width of the monochromator rocking curves in the vertical plane was unexpectedly large (see Table 1).

2.2. *The four-crystal- (4C-) monochromator configuration*

The mechanical design of the four-crystal monochromator used as a monochromator was based on the coupled rotation of two Si (111) channel-cut crystals driven by a translation stage. It has shown good stability and accuracy (Tolentino & Rodrigues, 1992; Tolentino, Durr, Mazzaro, Udron & Cusatis, 1995).

The incident energy in the back-diffraction condition for the Si 444 reflection of the thin plate (E = 7.91 keV corresponding to $\lambda = 2d_{444}$) was selected by the 333 reflection of the 4*C* monochromator set at a Bragg angle of 48.6°. In this configuration, among all the harmonics leaving the 4*C* monochromator, only the 333, 999, 12,12,12 *etc.* could be back diffracted by the plate. The fundamental 111 and the other harmonics (444, 555, ...) were not diffracted by the plate but transmitted with normal absorption.

Table 1. *Full width at half-maximum (FWHM) of the Si hhh rocking curves in the vertical plane for the 2C monochromator set at* $\theta = 88.95°$

Experimental values are compared with calculated widths ω (convolution of the Darwin width ω_D assuming, respectively, an angle φ equal to 0 and 0.8° in the perpendicular plane).

Harmonic	444	555	777	888	999
Energy (keV)	7.9	9.9	13.8	15.8	17.8
Experimental FWHM ('')	80	48	38	37	32
Calculated ω ('') with $\varphi = 0°$	54	16	4	3	1
Calculated ω ('') with $\varphi \simeq 0.8°$	84	46	34	33	31

With a dispersive four-crystal monochromator, the divergence of the outgoing beam in the diffraction plane (here the vertical plane) is of the same order of magnitude as the Darwin width. In the plane perpendicular to the diffraction plane (here the horizontal plane), the divergence of the outgoing beam is equal to the incident divergence. For the Si 333 reflection of the 4*C* monochromator, the actual angular divergence was around 0.005 (*V*) × 1.0 mrad (*H*).

3. Experimental results and discussion

Fig. 2 shows the *h*-beam and *o*-beam diffraction profiles for different temperatures of the thin plate, registered with the ionization chamber and the scintillation detector in the 2*C*-monochromator configuration. For diffraction angle sufficiently far from 90°, two back-diffracted

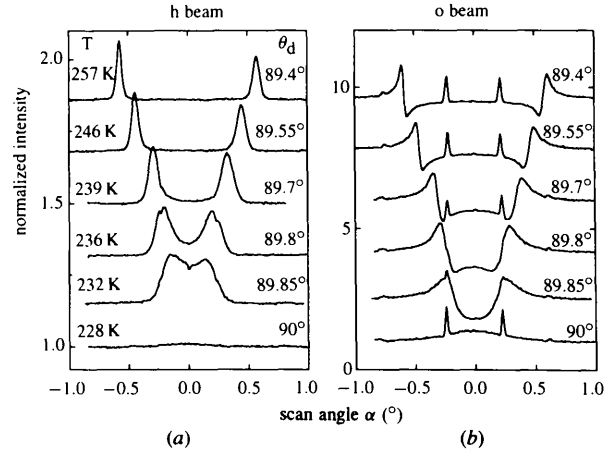

Fig. 2. (*a*) *h*-beam and (*b*) *o*-beam profiles measured simultaneously at different temperatures of the thin Si (111) plate, using the 2*C*-monochromator set-up (the curves are shifted on the vertical scale for clarity). The temperature and diffraction angle θ_d are indicated for each profile.

h-beam peaks are observed, corresponding to the two equal incidence angles θ and $(90° - \theta)$. The two peaks add to the nearly constant background due to the incident-beam intensity. The background of the h-beam profile was corrected for the decrease of the incident-beam intensity due to the lifetime of the positron current in the DCI ring. Then the profile was normalized to 1 in the region far from the peaks, where no diffraction occurs. Similar correction and normalization was done for the o-beam profiles.

From the measurement of the small angular separation of the two h-beam diffraction peaks, the diffraction angle could be determined with high precision. The diffraction angle measured at room temperature was equal to 88.95°. The thermal load on the first crystal of the $2C$ monochromator was negligible; the difference of temperature between the first and the second crystal was certainly lower than 5 K [that gives, according to (1), a difference between the Bragg angle of the two crystals lower than 0.04°]. Since the reflections were the same for the $2C$-monochromator crystal and the Si plate, the diffraction angle of the monochromator was also about 88.95°. The normal-incidence condition (90° diffraction angle) corresponds to the center of the angular distance between the two peaks. The absolute value of this angle did not change for angular scans performed at different plate temperatures. By lowering the temperature, the mean diffraction angle θ_d moved closer to 90°. The plate temperature was stabilized to within 1 K, resulting in an error on θ_d equal to 0.01° at $\theta_d = 88.95°$ and 0.05° at 89.85°.

Once the temperature is known with a precision of 0.1 K, the diffracted wavelength can be easily determined with good accuracy from the small angular separation between the two near-back-diffraction peaks, using the precisely measured lattice parameter of silicon (Seyfried *et al.*, 1992).

3.1. *The h-beam profiles*

The more important characteristics of the h-beam diffraction profiles are the rapid increase of its asymmetry and angular width when θ_d moves toward 90° until the two diffraction profiles merge. Then, for $\theta_d \simeq 90°$, the diffraction profile totally disappears because $2d_{hhh}$ is smaller than any incident wavelength λ.

Another characteristic of the experimental h-beam profiles is that systematically the reflectivity of one of the two diffraction peaks is smaller and the angular width larger than for the other one. This is a typical behavior of diffraction profiles in a dispersive/non-dispersive configuration. Nevertheless, since the diffraction plane of the monochromator, where the maximum angular dispersion of the narrow energy band leaving the $2C$ monochromator occurs, is the vertical plane, such behavior is not expected for angular scans of the thin plate in the horizontal plane. The difference between the two profiles observed in horizontal scans may be attributed to a small misalignment of the $2C$ monochromator relative to the incident white beam. If the horizontal axis of the monochromator is not set exactly perpendicular to the incident white beam, it will introduce an asymmetric energy dispersion in the horizontal plane. This asymmetry of the energy dispersion will be shown on the horizontally scanned back-diffracted profiles due to the high energy dispersion in this diffraction regime. This behavior could be used to check the alignment of high energy resolution $2C$ or $4C$ monochromators. For a monochromator set at a Bragg angle close to 90°, this misalignment is critical: for example, if the horizontal axis of the $2C$ monochromator set at a Bragg angle of 89° is not normal to the incident beam by 1°, the diffraction plane defined by the first crystal of the monochromator, where the maximum of the dispersion of the incident beam occurs, is no longer the vertical plane but the horizontal plane.

Table 2. *Contributions of the Si hhh harmonics to the total intensity of the transmitted beam, far from any diffraction, and to the incident beam taking the 444 contribution as unity, when the 2C-monochromator set-up was used (see text)*

The 333 contribution to the incident beam was calculated considering the absorption by air and by beryllium and the intensity in the DCI emission spectra for the 333 and 444 harmonics.

Harmonic	333	444	555	777	888	999
Energy (keV)	5.9	7.9	9.9	13.8	15.8	17.8
Transmitted beam	–	1	0.5	0.05	0.02	–
Incident beam	<0.1	1	8×10^{-3}	5×10^{-5}	1.2×10^{-5}	–

From the spectral composition of the transmitted o beam, it was deduced that the main contribution to the h-beam total diffraction profile was the 444 harmonic. The spectral composition of the o beam was obtained from the intensity of the background in the purely transmitting/absorbing angular region far from the diffraction peaks, using a solid-state detector. The relative intensity of each harmonic in the incident beam was then evaluated from the o-beam spectral composition, correcting each harmonic for the absorption on the 380 μm Si plate and on the Al foils in front of the solid-state detector (see Table 2).

With the $2C$ monochromator, the contrast of the diffraction peaks, defined here as the ratio between the height of the diffraction peak relative to the background and the total intensity of the peak, $(I_{\text{peak}} - I_{\text{background}})/I_{\text{peak}}$, was around 20% for the 'less-dispersive' peak (13% for the 'more-dispersive' peak). The actual contrast, when taking into account the absorption by air, at the energy of the 444 harmonic, inside and outside the ionization chamber, which is lower for the incident beam than for the h beam, was around 35% (25% for the 'less-dispersive' peak).

In Fig. 3, the measured FWHM of the *h*-beam diffraction peak is plotted against the diffraction angle for the 'less-dispersive' and the 'more-dispersive' sides. Two characteristics of the back-diffraction regime are responsible for the increasing of the *h*-beam peak angular width: the Darwin width becomes very large and the energy sensitivity (dispersion) is enhanced when the diffraction angle is approaching 90°.

Besides the increase of the angular width of the diffraction peak, both the 'more-dispersive' and the 'less-dispersive' profiles show an increasing asymmetry when the mean incidence angle approaches 90°: the higher-angle side is wider than the smaller-angle side. There are at least three possible origins for this asymmetry:

(*a*) owing to absorption, it is known from the dynamical theory that the intrinsic profile for each incident energy is asymmetric and the maximum of the profile is shifted toward the small-angle side;

(*b*) the Darwin width varies very rapidly for diffraction angles approaching 90°, and consequently is not constant for all the energies of the incident energy band;

(*c*) the energy dispersion, or energy sensitivity, increases very rapidly when the incidence angle approaches 90°. Therefore, the high-energy side of the incident energy band is diffracted in an angular region narrower than the low-energy side, and this should add a supplementary asymmetry in the total diffraction profile.

3.2. *The o-beam profiles*

The *o*-beam profiles are almost complementary to the *h*-beam profiles. The forward-diffraction profile is sensitive to the thickness of the thin plate. Far from the diffraction region, the incident beam is attenuated by the normal absorption. In the diffraction region, the profile of the *o*-beam peak is defined by the Borrmann effect.

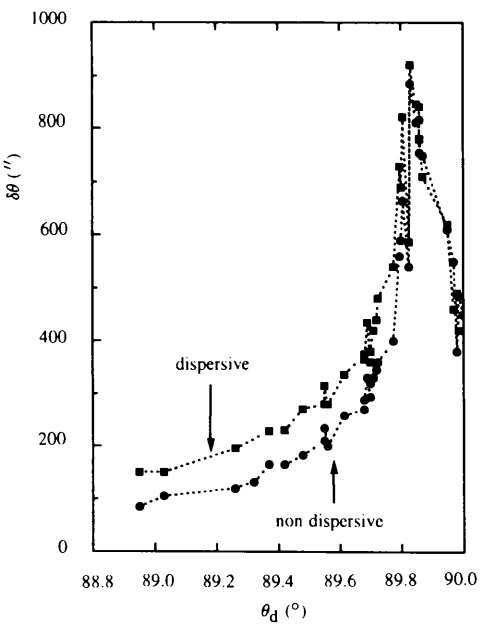

Fig. 3. Experimental FWHM of the 'non-dispersive' and the 'dispersive' profiles of the *h* beam.

In the *o*-beam profile with the mean diffraction angle at $\theta_d \simeq 89.4°$ (Fig. 2*b*), two unexpected peaks are observed at around 0.23° from the normal incidence position, between the two forward-diffracted peaks. No corresponding feature is observed in this region for the corresponding *h*-beam profile. These two extra peaks are not temperature sensitive and persist at the same angular position when the temperature is decreased (for θ_d approaching 90°). This strongly suggests that these features are not back-diffraction profiles. Other small peaks, which are also not temperature sensitive, can be observed at around −0.76, +0.62° and at exact normal incidence.

The occurrence of simultaneous diffraction follows a very simple rule for 90° diffraction and for an *hhh* reflection. The wavelength λ_{hhh} satisfying the back-diffraction condition for the *hhh* reflection will also be diffracted by the plane $(h'k'l')$ at a Bragg angle $\theta_{h'k'l'}$ when the angle β between the planes $(h'k'l')$ and $(\bar{h}\bar{h}\bar{h})$ is the complement of $\theta_{h'k'l'}$. For back diffraction, Bragg's law gives $\lambda_{hhh} \cong 2d_{hhh}$. Then, the relation of the h', k', l' Miller indices of the reflection in simultaneous diffraction condition with the *hhh* Miller indices of the back-diffracting reflection for a cubic crystal is

$$|\mathbf{h}| = (h'^2 + k'^2 + l'^2)/|h' + k' + l'| \qquad (2)$$

and $\theta_{h'k'l'}$ is given by

$$\theta_{h'k'l'} = \arcsin[(h'^2 + k'^2 + l'^2)/3h^2]^{1/2}. \qquad (3)$$

If $\theta_{h'k'l'}$ is smaller than 45°, the simultaneous diffraction occurrence corresponds to an asymmetric Laue case, otherwise, it corresponds to an asymmetric Bragg case. In any case, the *o* beam of the $h'k'l'$ reflection will contribute to the forward-transmitted-beam profile. Then, it is possible to associate any extra peak detected in the forward-diffracted profile with the *o* beam of an $h'k'l'$ simultaneous reflection.

The other planes diffracting simultaneously when the *hhh* harmonics are being diffracted at 90° are listed in Table 3 (it is not possible to have planes simultaneously diffracting when the 111 back-diffraction condition is satisfied). In these experiments, the main contribution to the *o* beam was due to the 444 and the 555 harmonics. For these wavelengths, simultaneous diffraction by the (400), (440), (53$\bar{1}$) and (620) planes was expected near 90°.

The extra peaks were observed for an incidence angle slightly different from 90° (−0.76, +0.62 and ±0.23°). This difference could be attributed to a slight misalignment of the plate in the vertical plane (this misalignment was estimated to be smaller than 1 mrad).

Table 3. *(hkl) simultaneous diffraction occurrences in the back diffraction of the Si hhh harmonics*

hhh reflection	$(h'k'l')$ plane	$h'^2 + k'^2 + l'^2$	$\theta_{h'k'l'}$ (°)
333	$(11\bar{1})$	3	19.47
	(422)	24	70.53
444	(400)	16	35.26
	(440)	32	54.74
555	$(53\bar{1})$	35	43.09
	(620)	40	46.91
777	$(64\bar{2})$	56	38.11
	(931)	91	51.89
888	(800)	64	35.26
	(880)	128	54.74
999	$(5\bar{1}\bar{1})$	27	19.47
	$(82\bar{2})$	72	32.98
	(11,7,1)	171	57.02
	(10,10,4)	216	70.53
	(12,6,6)	216	70.53

The exact harmonic composition of the extra peaks was only measured in the 4*C*-monochromator set-up and the *o*-beam profiles were detected separately for each harmonic. From this measurement (Fig. 4), it is then possible to identify the harmonic composition of the simultaneous diffraction peaks and the *o*-beam back-diffraction profiles.

Finally, using the two-crystal monochromator set-up, the *o*-beam profile maximum contrast varied between 37.5 and 50% for diffraction angles between 89.4 and 89.8°. Using the four-crystal monochromator set-up, the contrast was around 20% (the only diffracted harmonic was the 444 one). For each harmonic, it depends on the diffraction angle, the divergence and spectral composition of the incident beam and on the μt value, where μ is the linear absorption coefficient and t the plate thickness. For a 380 μm Si plate, μt varies between 6 for the 444 harmonic and 0.5 for the 999 harmonic. A higher contrast is expected if a thicker plate is used. In that case, a highly monochromatic beam in the incident direction would be obtained with the great advantage of solving the problem of the separation of the monochromatic beam from the incident beam in back-diffracting set-ups.

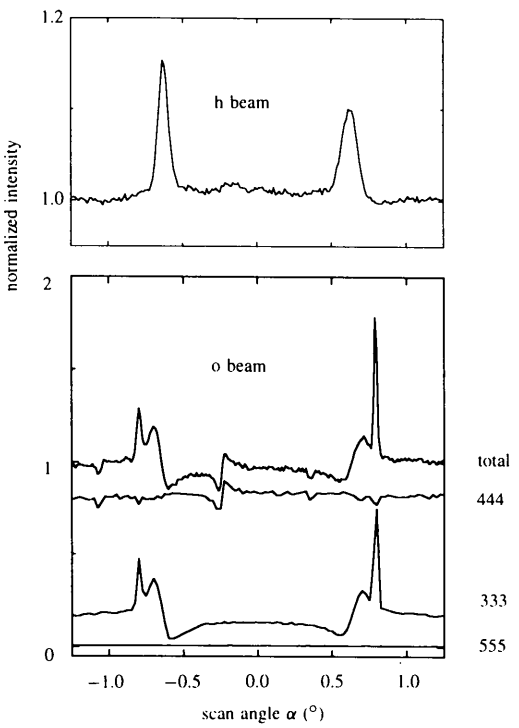

Fig. 4. *h*-beam profile and harmonic composition of the *o* beam registered with the solid-state detector in the 4*C*-monochromator configuration. Only the 333 4*C*-monochromator harmonic was back diffracted, the other harmonics (444 and 555) were purely transmitted by the plate.

4. Conclusions

An experimental study of the X-ray back-diffraction regime in an Si (111) plate with synchrotron radiation was realized using a set-up that enables the simultaneous measurement of the *o*-beam and the *h*-beam profiles at exactly 90°. The use of a solid-state detector allowed the analysis of the harmonic composition of the forward-diffracted beam. Using this set-up with a four-crystal monochromator, it is possible to characterize the back-diffraction region for any crystal reflection. An important question that remains unstudied up to now is the back-diffraction regime in mosaic crystals. The set-up presented in this paper could be used, for example, to confirm if the very large diffraction profiles of mosaic crystals also preserve the high energy resolution of the perfect crystals.

In the back-diffraction regime, the dynamical theory predicts extremely large Darwin widths and great energy sensitivity. It can be used to obtain highly monochromatic beams with higher intensity and using a goniometry much less sensitive to mechanical vibrations or thermal fluctuations than in the case of diffraction at angles far from 90°. Experimental *h*-beam and *o*-beam profiles have been measured for incidence angles θ from 89 to 90°. Some characteristics of the experimental profiles, such as the 'dispersive/non-dispersive'-like asymmetry of the *h*-beam and *o*-beam profiles and the extra features observed in the *o*-beam rocking curves, assigned here to simultaneous scattering extra peaks, deserve complementary studies. The good contrast of the *o*-beam profiles suggests that the back-diffracted *o* beam in a thick crystal could be used as a highly monochromatic beam and may result in an interesting way to overcome the experimental difficulties when using optics based on back diffraction.

We thank the LNLS staff for collaboration and assistance with the electronic control system (LOCO), operating programs and the monochromator construction and testing. We acknowledge the helpful support

and incentive of Dr Alain Fontaine (LURE) for the experimental realization. Thanks are also due to the DCI ring operators and technical staff for their kind assistance. Financial support from CNPq is gratefully acknowledged.

References

Brümmer, O., Höche, H. R. & Nieber, J. (1979). *Phys. Status Solidi A*, **53**, 565–570.

Caticha, A. & Caticha-Ellis, S. (1982). *Phys. Rev. B*, **25**, 971–983.

Corrêa, M. C., Tolentino, H., Craievich, A. & Cusatis, C. (1991). *Rev. Sci. Instrum.* **63**, 896–898.

Denne, W. (1978). *Acta Cryst.* A**34**, 1028–1029.

Dorner, B., Burkel, E. & Peisl, J. (1986). *J. Nucl. Instrum. Methods*, A**246**, 450–451.

Giles, C. (1991) Ms degree thesis, Universidade Federal Paraná (UFPr), Brazil. To be published.

Giles, C. & Cusatis, C. (1991). *Appl. Phys. Lett.* **59**, 641–643.

Giles, C. & Cusatis, C. (1992). Proceedings of SPIE Annual Meeting, No. 1740, pp. 198–206.

Graeff, W. & Materlik, G. (1982). *Nucl. Instrum. Methods*, **195**, 97–103.

Hämäläinen, K., Kao, C.-C., Hastings, J. B., Siddons, D. P., Berman, L. E., Stojanoff, V. & Cramer, S. P. (1992). *Phys. Rev. B*, 46, 14274–14277.

Hämäläinen, K., Siddons, D. P., Hastings, J. B. & Berman, L. E. (1991). *Phys. Rev. Lett.* **67**, 2850–2853.

Hashizume, H. & Nakahata, T. (1988). *Jpn. J. Appl. Phys.* **27**, L1568–L1571.

Hofmann, W., Kalus, J. & Schmelzer, U. (1992). *J. Appl. Cryst.* **25**, 340–347.

Kohra, K. & Matsushita, T. (1972). *Z. Naturforsch. Teil A*, **27**, 484–487.

Kondrashkina, E. A., Novikov, D. V. & Stepanov, S. A. (1989). *Phys. Status Solidi A*, **121**, K9–13.

Kushnir, V. I. &. Suvorov, E. V (1986). *JETP Lett.* **44**, 262–265.

Kushnir, V. I. &. Suvorov, E. V. (1989). *Nucl. Instrum. Methods*, A**282**, 539–541.

Nakahata, T., Hashizume, H., Oshima, M. & Kawamura, T. (1989). *Jpn. J. Appl. Phys.* **28**, L300–L303.

Schülke, W. (1989). *Nucl. Instrum. Methods*, A**280**, 338–348.

Sette, F. (1993). ESRF Annual Report. ESRF, Grenoble, France.

Seyfried, P., Becker, P., Kozdon, A., Lüdicke, F., Spieweck, F., Stümpel, J., Wagenbreth, H., Windisch, D., De Bièvre, P., Ku, H. H., Lenaers, G., Murphy, T. J., Peiser, H. S. & Valkiers, S. (1992). *Z. Phys. B*, **87**, 289–298.

Stepanov, S. A., Kondrashkina, E. A. & Novikov, D. V. (1991). *Nucl. Instrum. Methods*, A**301**, 350–357.

Stetsko, Yu. P., Kshevetskii, S. A. & Mikhailyuk, I. P. (1988). *Sov. Phys. Tech. Phys. Lett.* **14**(1), 13–14.

Steyerl, A. & Steinhauser, K. A. (1979). *Z. Phys. B*, **24**, 221–227.

Tolentino, H., Durr, J., Mazzaro, I., Udron, D. & Cusatis, C. (1995). *Rev. Sci. Instrum.* **66**, 1806–1808.

Tolentino, H. & Rodrigues, R. D. (1992). *Rev. Sci. Instrum.* **63**, 946–949.

Woodruff, D. P., Seymour, D. L., McConville, C. F., Riley, C. E., Crapper, M. D., Prince, N. P. & Jones, R. G. (1987). *Phys. Rev. Lett.* **58**, 1460–1462.